PHYSICAL REVIEW B **79**, 224116 (2009)

First-principles calculations of defects near a grain boundary in MgO

K. P. McKenna* and A. L. Shluger
World Premier International Research Center, Advanced Institute for Materials Research, Tohoku University, 2-1-1 Katahira, Aoba-ku, Sendai 980-8577, Japan
and Department of Physics and Astronomy and London Centre for Nanotechnology, University College London, Gower Street, London WC1E 6BT, United Kingdom
(Received 23 April 2009; published 25 June 2009)

The electronic structure of oxygen vacancy and proton defects close to grain boundaries in MgO are calculated using first principles methods. These defects, in various charge states, favorably segregate to grain boundaries and can trap electrons. The interplay between electron and defect segregation provides a mechanism for charge to build up at boundaries, for example, under irradiation or applied electrical voltage. The theoretical calculations presented provide insight into the complex electronic properties of metal-oxide grain boundaries that can be difficult to obtain by experiment alone but which are important for many applications.

DOI: 10.1103/PhysRevB.79.224116 PACS number(s): 68.35.−p

I. INTRODUCTION

Polycrystalline metal-oxide materials find numerous technological applications where grain boundaries are known or suspected to influence functionality. Solid oxide fuel cells,[1–4] gas sensors,[5] thermal barrier coatings,[6] varistors,[7] high-T_c superconductors,[8,9] and metal-oxide-semiconductor field-effect transistors (MOSFETs) (Refs. 10 and 11) are just a few important examples. Grain boundaries in these systems can be both beneficial and harmful to applications and have been the subject of considerable research.[12] Perhaps the best characterized metal-oxide material in terms of grain boundaries is MgO, which is often considered as a model oxide system. A large number of experiments[13–19] using methods such as transmission electron microscopy (TEM) and radioactive tracer diffusion provide clear evidence that grain boundaries in MgO act as sinks for defects and impurities and also can provide shortcut paths for their diffusion. Theoretical calculations based on interatomic potentials[20–25] and density-functional theory (DFT) (Ref. 13) also support these results. However, an issue that has received little attention so far is that defects segregated to grain boundaries may exist in one of several charge states. Furthermore, during device operation or in an experiment processes, such as electron irradiation, optical excitation, or electrical injection, may modify the charge state of defects through electron or hole trapping, significantly modifying their properties. A detailed understanding of such effects requires the characterization of the electronic properties of defects at grain boundaries, and this has so far been lacking.

In this paper, we tackle this problem by using a first principles embedded cluster method to investigate the electronic properties of defects segregated to a grain boundary in MgO. Two important types of defects, proton impurities and oxygen vacancies, are considered and their properties at the grain boundary are compared to those in the bulk and at the (001) surface. Oxygen vacancies are considered as they are almost always present in metal oxides, either because they are underoxidized or because they are intentionally introduced by doping (e.g., as in O-ion conductors such as yttria stabilized zirconia). Similarly, protons can be easily introduced since water vapor is almost always present during growth.[14] Our methodology is demonstrated on a tilt grain boundary in MgO, which represents a useful model system for several reasons. First, MgO has many applications where defects and associated charge trapping can play an important role, for example, it is widely used as an insulating barrier in tunneling magnetoresistive junctions,[26] a secondary electron emitter for flat panel displays,[27] and a substrate for thin films and metallic clusters.[28] It has been suggested that charge trapping at grain boundaries is responsible for dielectric breakdown in MgO,[29] and this has also been suggested for other oxides such as HfO_2.[10,11] Another reason for choosing MgO is that, as described above, the structure and dynamics of tilt grain boundaries in MgO have been studied in some detail. Interestingly TEM, which is commonly used to image boundaries, is itself a source of electrons and irradiation has been observed to induce motion of grain boundaries in MgO.[30] Finally, the embedded cluster method we employ has been well tested for MgO through previous studies of defects on MgO surfaces,[31–34] which should allow us to make quantitative predictions.

Our calculations show that both protons and oxygen vacancies favorably segregate to grain boundaries in MgO. We also find that vacancies and protons combine at the boundary to form stable defects that can exist in a number of different charge states. On electron trapping many of these defects undergo reactions which lead to the production of hydrogen molecules. The formation energies and electronic properties of these defects have been calculated using an embedded cluster method and compared to those of defects in the bulk and on the MgO surface. The approach that we employ is described in detail in this paper, and it represents an advance over previous interatomic potential methods as it is not restricted to studying defects in only a single charge state. While this paper addresses defects in MgO, the methodology that is described can also be employed to study other technologically important metal-oxide systems, such as zirconia and hafnia, where space charge and electron trapping at boundaries can be important for fuel cell operation and dielectric breakdown in transistors.[11]

The rest of this paper is organized in the following way. In Sec. II we briefly review what is known about the struc-

ture and electronic properties of grain boundaries in MgO. Then in Sec. III we describe the methods we employ to address these problems theoretically before presenting our results in Sec. IV. Finally the results are summarized and discussed in Sec. V, where connections to experiment and applications are also highlighted.

II. BACKGROUND

When attempting to understand the properties of polycrystalline materials, whether experimentally or theoretically, one is faced with the problem that real materials usually contain a variety of different boundary structures. Various factors, including the presence of impurities, ambient gas pressure, and thermal treatment, influence both the types of boundary present and their relative concentration. However, it is intuitively expected that boundaries with low energies of formation and a high degree of lattice coincidence between grains are more prevalent in real systems. This expectation is supported by experimental studies of grain orientations in polycrystalline MgO, and also for many other materials, by methods such as x-ray diffraction, backscattered electron diffraction,[35] and TEM. While it is difficult to extract detailed models of the atomic structure of grain boundaries from experiments on polycrystalline systems, atomically resolved images of the boundary structures in MgO have been obtained using TEM on bicrystals.[13,36] Given the experimental challenges involved in characterizing grain boundary structures, theoretical modeling plays a particularly important role. In previous studies a range of tilt[21,22,37] and twist boundaries[38] in MgO have been modeled using atomistic methods and the predicted stable boundary structures are in good agreement with experiment. Atomistic simulations have also shown how edge dislocations of the sort found in tilt grain boundaries can form in thin MgO films to accommodate the lattice mismatch of a support.[23]

Defects and impurities in polycrystalline materials favorably segregate grain boundaries driven by both local variations in electrostatic potential and decreased density at the boundary (which allows for more structural relaxation).[16] It has been shown how impurities that segregate to boundaries can transform their structure locally, e.g., as seen for Ca impurities in MgO.[13] Segregated impurities can also affect the creep behavior of polycrystalline materials by modifying barriers to grain boundary sliding, e.g., as demonstrated recently for alumina.[39,40] The formation energies of intrinsic defects in MgO, such as Frenkel and Schottky, are too high to be present in significant concentrations at room temperature. However, extrinsic defects can be present in order to compensate for the charge of aliovalent impurities. In MgO, typical impurity concentrations are on the order of hundreds of parts per million[41] (ppm). Experimental methods such as TEM, radioactive tracer diffusion,[18] and conductivity measurements[14,15,19] provide strong evidence for defect segregation in MgO. Theoretical models describing defect segregation and the associated space charge that forms in equilibrium can be used to interpret these experiments.[42–50] Advanced scanning probe microscopies can be used to directly measure the nanoscale variations in electric potential in oxide bicrystals that are produced by space charge.[51,52] The space charge associated with grain boundaries in MgO has also been measured by electron diffraction which is sensitive to inner potential variation near grain boundaries.[53] Experimental studies have been complemented by extensive atomistic simulations focusing on defect segregation and diffusion near MgO grain boundaries.[20–25]

The electronic properties of grain boundaries and their associated defects and impurities can be probed using a range of techniques such as energy dispersive x-ray spectroscopy, electron-energy-loss spectroscopy,[9,13] auger electron spectroscopy,[16,17] transport measurements,[54] and scanning tunneling spectroscopy (STS).[10,55] Localized electronic defects at boundaries, such as the F^+ center in MgO (which is an O vacancy with one trapped electron), can also be studied using methods such as electron paramagnetic resonance (EPR).[56] In general, quantum mechanical calculations of the electronic structure of grain boundaries in oxide materials are relatively uncommon. Previous studies include MgO,[38,57] TiO_2,[58] alumina,[59] $SrTiO_2$,[60,61] ZnO,[62] and HfO_2.[63] Calculations of the electronic properties of defects at grain boundaries and their ability to trap charge have so far been missing.

III. COMPUTATIONAL METHODS

A. Atomistic methods

As the first component of a hierarchical methodology we employ empirical interatomic potentials to model the structure of grain boundaries. The relative computational simplicity of interatomic potentials, e.g., as compared to DFT means that large numbers of candidate structures can be generated and the most probable selected on the basis of formation energy. For MgO we use the empirical polarizable shell model potentials of Lewis and Catlow,[64] which have been shown to accurately reproduce many physical properties. To determine the atomic scale structure of a grain boundary for a given misorientation angle we employ the METADISE code which is described fully in Ref. 37. Briefly, the idea is to construct a two dimensionally periodic interface between two grains which are oriented at prescribed angles. The grains are modeled with periodic boundary conditions parallel to the interface and sufficiently wide in the perpendicular direction that relevant properties of the interface are converged (i.e., the electrostatic potential, interface formation energy, and structure). Ions near to the interface (within 30 Å) are free to relax while more distant ions are held fixed at their bulk positions. To fully optimize the structure of the boundary, the energy is minimized with respect to the positions of ions near the interface, lateral translations, and intergrain dilations and also the addition and removal of ions at the interface. Atomistic methods can provide accurate models of grain-boundary structure, and they can also be used to model the properties of some types of defects (e.g., impurities and charged vacancies). However, to model the electronic properties of grain boundaries and those of associated defects, which may involve electrons or holes, one must turn to a quantum mechanical description.

B. Embedded cluster method

Defects in ionic systems, especially charged ones, can induce long-range polarization of the surrounding ions. How-

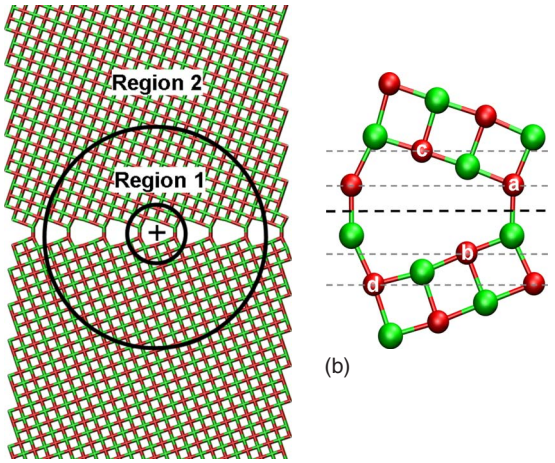

FIG. 1. (Color online) (a) The (310)[001] tilt grain boundary in MgO modeled using the embedded cluster method. The extent of regions 1 and 2 and the location of the quantum cluster are indicated. (b) The 54 atom quantum cluster that is embedded at the grain boundary. Inequivalent anion sites near the boundary are also labeled a–d (see text). Color scheme: oxygen ions are dark (red online) and magnesium ions are light (green online).

ever, periodic quantum-mechanical calculations are restricted to relatively small systems and cannot capture this effect in calculations of their electronic properties. The philosophy behind the embedded cluster approach is that, as the electronic states of defects are usually well localized, one can divide the system into a small part that is modeled quantum mechanically and a larger part that is treated at an empirical potential level. This type of approach is implemented in the GUESS code, which has been applied previously to model the MgO surface[31,32,65–71] and recently to model interfaces between MgO nanocrystallites.[34] In this paper, an MgO grain boundary is modeled as an interface between two large grains (about 50 Å edge length) each containing 16 128 ions [Fig. 1(a)]. The bicrystal geometry is obtained from the atomistic optimization described above (Sec. III A). The setup is such that the charge dipole in all directions is negligible. The system is subdivided into two regions. In region 1, which extends 17 Å from the center of the bicrystal [indicated by the cross in Fig. 1(a)], all ions are free to relax. In region 2, ions are fixed in bulk positions. Most ions in the bicrystal are modeled using polarizable interatomic potentials, however, the ions closest to the center of the bicrystal are treated at a fully quantum mechanical level (quantum cluster). This quantum cluster [Fig. 1(b)] is described quantum mechanically using the GAUSSIAN03 code. The quantum cluster is treated at an all-electron level using the B3LYP hybrid density functional.[72,73] The improved treatment of exchange provided by B3LYP is needed to obtain quantitatively correct results for the band gap of MgO (Ref. 74) and for the properties of various defects, e.g., optical absorption and electron paramagnetic resonance g tensors. As in previous studies,[31,32] we used the standard Gaussian 6-31G basis set on Mg and O ions, but have extended the basis to 6-311 $+G^*$ on low-coordinated atoms and on protons we have used a 6-311$+G^{**}$ basis set. Mg ions surrounding the quantum cluster (within 5 Å) are modeled using a semilocal effective core pseudopotential which prevents spurious spilling of the wave function from the quantum cluster into the classically modeled regions. The total energy of the quantum cluster, in the electrostatic potential produced by all surrounding classical ions, is calculated by solving the Kohn-Sham equations. The forces acting on all ions in region 1 are then calculated and the geometry of the entire system is optimized self-consistently using the BFGS algorithm.

The main disadvantage of the embedded cluster method is that it is not suited to modeling electronic states that are delocalized over relatively large regions of the system (e.g., bulk conduction and valence-band states). Therefore, properties that depend on these states, such as the bulk band gap, exhibit a dependence on the quantum cluster size. To obtain accurate results one must examine the cluster size dependence and extrapolate to infinite size. If this is carried out for bulk MgO using quantum clusters of sizes 27, 48, and 64 atoms, the extrapolated bulk band gap is obtained as 7.8 eV—very close to the experimental value. For states that are well localized inside the quantum cluster, e.g., core levels or F centers, the results are less sensitive to the cluster size.

C. Periodic quantum mechanical methods

Periodic quantum-mechanical approaches using DFT, for example, are much more appropriate for modeling delocalized electronic states and provide an important third component to our methodology. They also allow us to check the consistency of the boundary conditions employed in the embedded cluster calculations. Starting from the classically optimized grain boundary structure a three-dimensional periodic supercell is constructed. The supercell must be chosen to be sufficiently large to ensure that the electrostatic and elastic interaction between boundaries is negligible. We then employ periodic DFT calculations using the projector-augmented wave method[75] and the Perdew-Burke-Ernzerhof (PBE) functional as implemented in the VASP code.[76,77] We use only a single k point (the gamma point) and plane waves with energies up to 400 eV. Atomic coordinates and cell dimensions are optimized to within a force tolerance of 0.01 eV Å^{-1}.

IV. RESULTS

There are a large number of different high coincidence boundaries in MgO but we restrict the discussion here to the (310)[001] (36.8°) tilt grain boundary. We have considered other structures, but find that the interesting features of the electronic structure are connected to the dislocation core itself and the (310) boundary serves as a suitable example.

A. Pristine MgO (310)[001] tilt grain boundary

We first discuss the properties of the pristine tilt grain boundary in MgO, which provides a reference for the defective boundaries we consider in the following sections. Using the METADISE code, we find that the most stable structure of the (310) boundary has no rigid body translation and involves an array of equally spaced dislocation pipes as shown

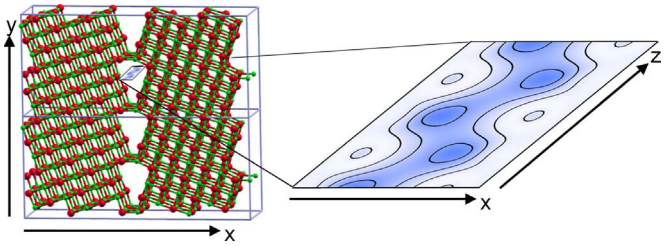

FIG. 2. (Color online) (Left) The periodic supercell used to model the (310)[001] (36.8°) tilt grain boundary in MgO. (Right) The charge density isosurface for an electron trapped inside the dislocation core at the boundary (see text for discussion). Darker color represents higher electron density.

in Fig. 1. A periodic supercell containing 120 ions and two grain boundaries (cell dimensions $13.35 \times 8.33 \times 28.96$ Å) has also been constructed and is shown in Fig. 2. The geometry of the supercell is fully optimized by periodic DFT with cell dimensions parallel to the interfaces fixed at their bulk values. The optimized cell has boundaries separated by nearly 15 Å. The formation energy for the (310)[001] boundary is calculated to be 1.95 J m^{-2} with respect to the bulk, agreeing rather well with previous calculations using atomistic methods.[37]

Figure 3 shows the electronic density of states (DOS) calculated using periodic DFT together with the bulk DOS as a reference. To separate bulk and interface contributions to the electronic structure, the charge density associated with individual electronic states is calculated and their spatial distribution is analyzed, as described in Ref. 57. While there is only a small splitting (<0.1 eV) of occupied interface states from the top of the valence band, two sets of unoccupied states, labeled Δ_I and Δ_{II} in Fig. 3, are more significantly split from the bulk conduction band which starts just below 5 eV.

The interface state Δ_I is located 1 eV below the bulk conduction-band minimum, therefore, the interface presents a trap for conduction-band electrons. Analyzing the spatial

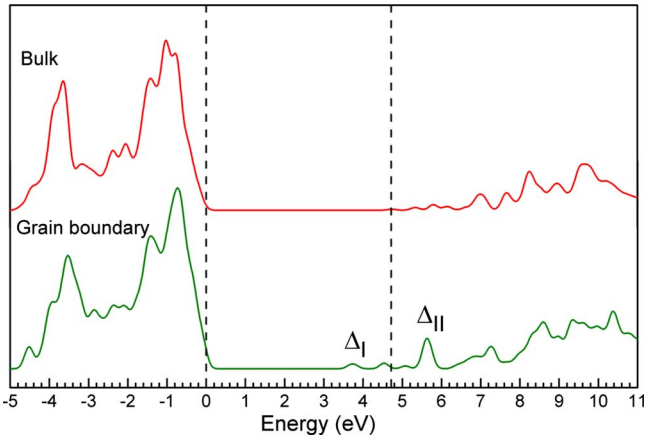

FIG. 3. (Color online) DOS of the tilt grain boundary in MgO together with the bulk DOS as a reference. The dashed lines indicate the positions of the bulk valance-band maximum and conduction-band minimum. States associated with the grain boundary are labeled Δ_I and Δ_{II}.

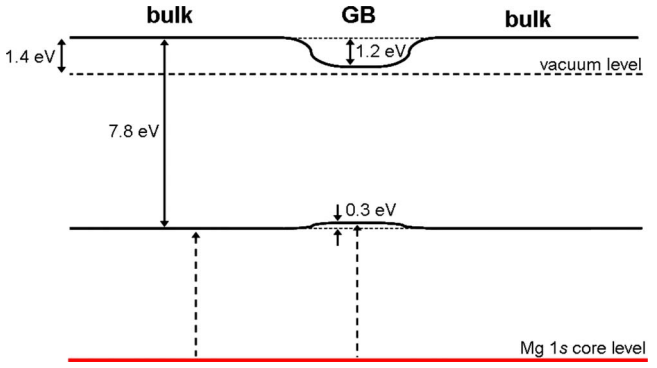

FIG. 4. (Color online) The electronic structure of the (310)[001] grain boundary determined by the embedded cluster method. The bulk and grain boundary electronic structures have been aligned using the core Mg 1*s* states as a common reference, Ref. 79. The vacuum level is shown by the dashed line and is calculated from the ionization energy of the (001) surface. The results indicate that boundaries present a shallow trap for valence-band holes but a deep trap for conduction-band electrons.

distribution of a trapped electron (using Bader analysis[78]) we find that, unusually, the electron is primarily (about 80%) located *inside* the dislocation core. The remaining 20% is attributed to nearby anions and this density is strongly polarized toward the center of the core. Examining electron-density isosurfaces for a cut plane through the dislocation core (Fig. 2), the quasi-one-dimensional form of the electron localization is revealed. The confined electron snakes its way down the center of the dislocation cores, following the weakly attractive electrostatic potential of Mg^{2+} ions on the internal surfaces. The grain boundary also introduces resonant states in the bulk conduction band (labeled Δ_{II} in Fig. 3). The higher energy of these states is explained by their association with the more confined part of the dislocation core.

As DFT underestimates the band gap of MgO, we have repeated these calculations using the embedded cluster method and the B3LYP functional. Separate quantum clusters were used to model the grain boundary, bulk, and surface properties. The electronic structures of these separate clusters are aligned using the average position of the core Mg 1*s* levels as a common reference, e.g., see Ref. 79. Figure 4 shows schematically how the electronic structure varies near a tilt grain boundary. The vacuum level is also indicated since we have been able to determine this by calculating the ionization potential of the surface quantum cluster.[31] The results are qualitatively similar to those obtained from DFT, namely, there is a small splitting of states from the valence band (0.3 eV) and a much larger splitting of interface states from the conduction band (1.2 eV). Weak hole trapping at interfaces in MgO is consistent with previous calculations of interfaces between MgO nanocubes in powders.[34] The spatial distribution of an electron trapped at the boundary is also qualitatively similar to that obtained by periodic DFT although the electron density has finite extension along the dislocation core due to the absence of basis functions outside the quantum cluster. Using the embedded cluster approach we have also calculated the optical excitation for the bound-

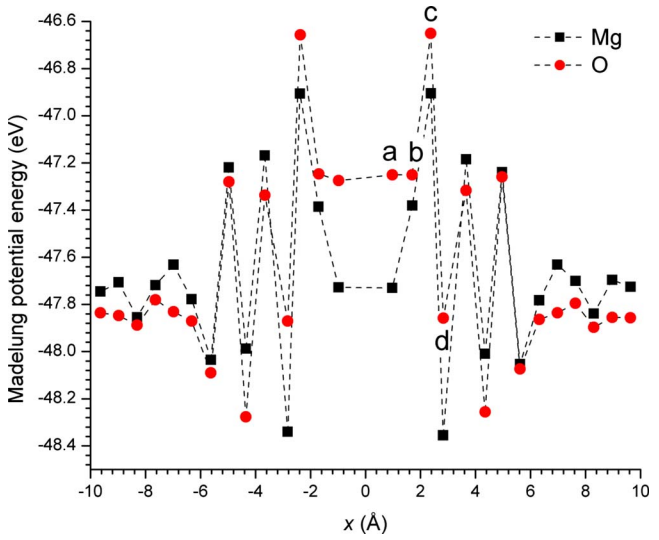

FIG. 5. (Color online) The electrostatic potential energy of Mg and O ions on either side of the grain boundary calculated in the center of the bicrystal. Anion sites close to the boundary are labeled a–d.

ary using TD-DFT. The maximum absorption dipole moment is at 6.0 eV and is directed perpendicular to the boundary plane [i.e., from top to bottom in Fig. 1(b)].

We note that these calculations show that MgO is a negative electron affinity (NEA) material, i.e., the bottom of the bulk conduction band lies above the vacuum level, in agreement with many-body *GW* calculations.[80] Comparing the PBE, B3LYP, and many-body *GW* calculations we find that the electron affinity (EA) of MgO is quite well predicted by PBE and slightly underestimated using B3LYP. The NEA of MgO is the key to understanding the origin of the unusual electron trapping at grain boundaries. This is because small channels and pockets of empty space that are found in many grain boundary structures can provide possible places for electrons to trap relative to the bulk conduction band. Whether this is energetically favorable depends upon the kinetic-energy cost associated with confining the electron. In a separate paper[57] we have discussed these effects in detail and also considered NaCl and LiF boundaries. We now consider processes involving the interaction of electrons with defects at grain boundaries.

B. Segregation and electronic properties of oxygen vacancies

Before discussing the properties of anion vacancy defects we examine the electrostatic potential energy for the bicrystal on which the embedded cluster calculations will be performed [Fig. 1(a)]. The electrostatic potential energy is calculated using formal ionic charges and the geometry obtained following optimization using classical interatomic potentials (Sec. III A). The potential is calculated for ions which are at least 15 Å from any of the exterior surfaces. In this region, variations in the potential within planes parallel to the boundary are less than 1% demonstrating that bicrystal is sufficiently large to eliminate edge effects. Figure 5 shows the electrostatic potential energy averaged over planes parallel to the boundary and its dependence on the distance from the boundary (x=0 Å). There are strong oscillations in potential with an amplitude of about 0.8 eV close to the boundary, however, the bulk Madelung potential is reached for sites more than about 10 Å from the boundary.

To characterize the tendency for defects to segregate to various sites at the grain boundary we calculate their formation energies. Four oxygen sites close to the boundary are considered, labeled a–d in Figs. 1(b) and 5, and we also calculate the properties of vacancies on the (001) surface as a reference. Anion vacancies in MgO containing zero, one, or two electrons are known as F^{++}, F^{+}, and F^{0}, respectively, and are found to be stable in the bulk, at the surface, and at the grain boundary. To determine which site and which charge state of the vacancy is most favorable, we calculate the vacancy formation energies with respect to oxygen and electron chemical potentials, μ_O and E_F, respectively. The formation energy is given by

$$E_f(\mu_O, E_F) = E^q_{defect} - E_{ideal} + \mu_O + qE_F, \quad (1)$$

where E_{ideal} is the total energy of the ideal system, E^q_{defect} is the energy of the defective system in relative charge state q, and E_F is measured with respect to the vacuum level. In these calculations we have taken $\mu_O = E_O = -2042.46$ eV (the energy of an oxygen atom in the triplet state). We also calculate,

$$E_s = E^{GB}_f - E^{Bulk}_f, \quad (2)$$

which is the segregation energy of the defect from the bulk and is independent of both μ_O and E_F. A negative value of E_s means that segregation from the bulk is energetically favorable. To calculate the bulk properties, a quantum cluster is embedded into the center of one of the crystallites, shown in Fig. 1(a), 15 Å away from the grain boundary.

Table I summarizes $E_f(E_O, 0)$ for each charge state of the vacancies. The calculations show that the two most stable sites for O vacancy segregation at the boundary are a and b, which have very similar formation energies and similar electrostatic potential energies (Fig. 5). We also compute the charge transition level, $\bar{\mu}$. It is defined as the electron chemical potential for which the formation energies of different charge states of the defect are equal.[79] For the F^0/F^+ charge transition we find $\bar{\mu} = -2.0$ eV in the bulk, $\bar{\mu} = -2.2$ eV at the surface, and $\bar{\mu} = -2.3$ eV for grain boundary sites a and b. As these charge-transition levels are different, the charge state of O vacancy defects depends upon their location.

The defect levels associated with the O vacancies at grain boundaries can be compared directly using the level alignment procedure based on Mg 1s states.[79] Figure 6 summarizes the positions of occupied and unoccupied one-electron levels for O vacancies in the bulk and at the most favorable grain boundary sites (i.e., a and b). One can see that anion defect levels at the grain boundary are qualitatively similar to those in the bulk, but are 0.3 eV lower in energy. This shift in energy correlates with the shift in charge transition level that has been calculated on the basis of total energies. It is also consistent with the 0.3 V difference in electrostatic potential for sites a and b compared to the bulk. This can be seen in

TABLE I. The formation energies for anion vacancy defects in the bulk, at the surface, and at various sites at the (310)[001] grain boundary (all energies are in eV). See Fig. 1(b) for the definitions of the defect positions.

F^0	Site	$E_f(E_O,0)$	E_s
	bulk	10.63	
	(001)	9.60	−1.03
	a	9.76	−0.87
	b	9.69	−0.93
	c	10.53	−0.10
	d	11.39	+0.76
F^+	Site	$E_f(E_O,0)$	E_s
	bulk	12.61	
	(001)	11.82	−0.80
	a	12.04	−0.57
	b	12.01	−0.60
	c	12.69	+0.08
	d	13.73	+1.12
F^{2+}	Site	$E_f(E_O,0)$	E_s
	bulk	16.33	
	(001)	16.14	−0.19
	a	15.96	−0.37
	b	15.99	−0.34
	c	16.58	+0.25
	d	17.88	+1.55

Fig. 5, noting that as the Madelung potential energy is shown in this figure one must divide by two to obtain the electrostatic potential. This consistency is strong evidence that the core level alignment procedure is correct. We also note that the one-electron energy difference between the occupied states of F^0 and the bulk conduction band is 5.1 eV. This is in good agreement with optical-absorption spectra which find F-center optical absorption at 250 nm (4.96 eV), as excitation energies are typically several tenths of an eV lower than single-electron level differences. From the position of these defect levels one can also conclude that optical properties of defects at tilt grain boundaries are different from the bulk, but quite similar to those of surface defects.

The g tensors for the paramagnetic F^+ defects have also been calculated to allow comparison with experimental EPR spectra (Table II). The calculations have been performed using the defect geometries obtained by the method described in Sec. III B, but with the basis increased to 6-311+G^{**} on all ions in the quantum cluster. We find that the g-tensor components are largest for F^+ in the bulk and smallest for F^+ at the (001) surface. For F^+ at the grain boundary g-tensor components are intermediate between surface and bulk. The values calculated for the surface are in good agreement with previous calculations.[81]

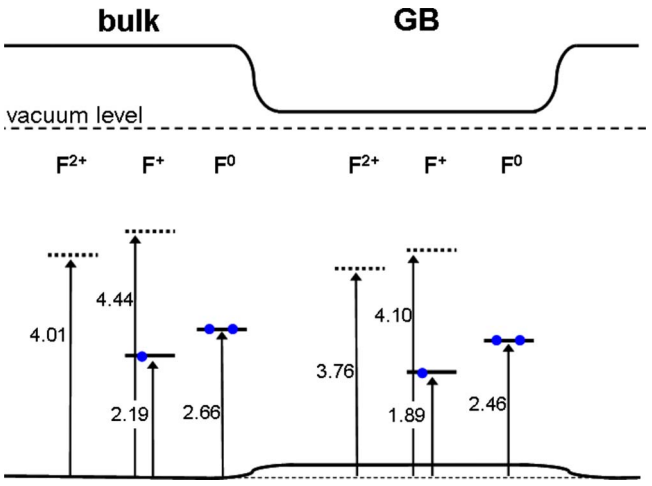

FIG. 6. (Color online) Electronic states of O vacancy defects in the bulk and at grain boundary sites a and b. Occupied (full lines) and lowest unoccupied levels (dashed lines) as given by the one-electron energies are shown together with their splitting from the bulk valence-band maximum measured in eV. Filled circles show the number of electrons in each occupied level.

C. Segregation and electronic properties of proton impurities

Protons are a common impurity in many oxide materials[14,82] and can be introduced by adsorption and dissociation of water or hydrogen on surfaces. They can also be incorporated during production of the material, for example, one way to obtain MgO is by decomposition of $MgOH_2$ (see Ref. 83 and references within). To determine whether proton related defects favorably segregate to grain boundaries in MgO, we have performed calculations of their formation energy and electronic properties. We have also investigated the interaction of protons with oxygen vacancy defects and the ability of proton defect configurations to trap additional electrons.

At the surface and in the bulk of MgO it is well known that protons bind to O^{2-} ions forming an hydroxyl group (OH^-).[82] However, at the grain boundary, not all oxygen ions are equivalent and there is the potential for more unusual proton configurations. Therefore, to find stable proton adsorption sites within the grain boundary we first generated a

TABLE II. EPR g tensors for paramagnetic defects.

F^+	Site	g_1	g_2	g_3
	bulk	2.00229	2.00229	2.00229
	(001)	2.00119	2.00121	2.00193
	b	2.00146	2.00154	2.00208
H	Site	g_1	g_2	g_3
	bulk	2.00280	2.00281	2.00287
	(001)	2.00047	2.00047	2.00247
	I	2.00031	2.00086	2.00130
	F_b^0	2.00094	2.00159	2.00210

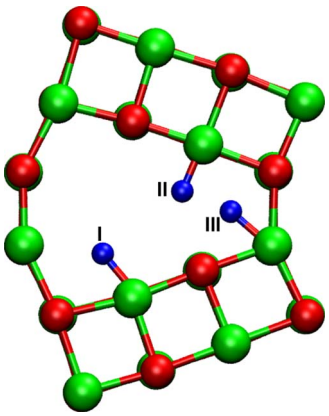

FIG. 7. (Color online) The quantum cluster embedded at the MgO grain boundary together with the three stable proton configurations (I–III).

number of initial configurations, chosen such that the position of the proton uniformly sampled the grain boundary region. Each of these configurations were then relaxed into local minima, many of which we found to be equivalent. At the end of the search we found three inequivalent adsorption sites, each involving binding of the proton to an O^{2-} ion, which we label I–III in Fig. 7. Configurations I and II resemble proton adsorption at the (001) surface. Configuration III is more unusual as it involves a proton that bridges between the two grains.

TABLE III. The formation energies for proton defects in the bulk, at the surface and at various sites at the (310)[001] grain boundary (all energies are in eV). See Fig. 7 for the definitions of the defect positions. The formation energy of proton defects are calculated with respect to a proton in vacuum (i.e., the proton affinity) and alternatively with respect to a H atom in vacuum.

p	Site	$E_f(0,0)$	E_s
	bulk	−11.17	
	(001)	−12.82	−1.65
	I	−12.95	−1.78
	II	−12.46	−1.29
	III	−11.56	−0.39
	F_b^{2+}	−5.97	+5.20
	F_b^{+}	−10.54	+0.63
	F_b^{0}	−15.45	−4.27
H	Site	$E_f(E_H,0)$	E_s
	bulk	+2.50	
	(001)	−0.43	−2.93
	I	−0.18	−2.68
	II	−0.06	−2.56
	III	+1.43	−1.07
	F_b^{2+}	−0.86	−3.36
	F_b^{+}	−4.10	−6.60
	F_b^{0}	−2.46	−4.96

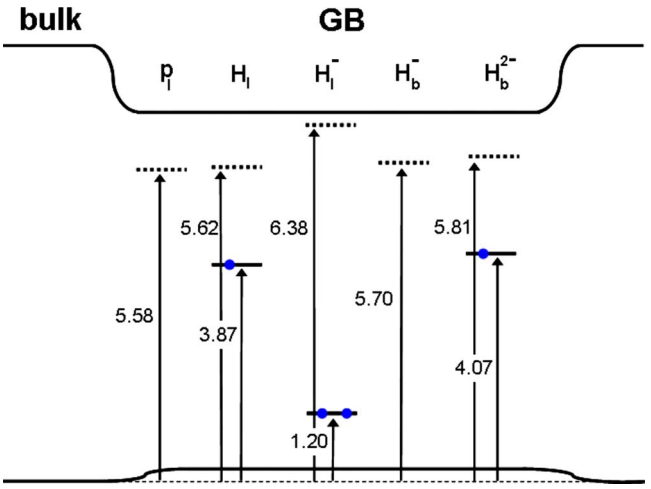

FIG. 8. (Color online) Electronic states of proton defects at grain boundary sites. Occupied (full lines) and unoccupied levels (dashed lines) as given by the one-electron energies are shown together with their splitting from the bulk valence-band maximum measured in eV. Filled circles show the number of electrons in each occupied level.

The formation and segregation energies for proton defects in the bulk, at the surface, and at the grain boundary are summarized in Table III and have been calculated with respect to the energies of a proton (i.e., the proton affinity) and a hydrogen atom in vacuum. To simplify the discussion of these defects it helps to consider a particular sequence of events involving the segregation of a proton to the grain boundary. We then discuss what happens when protons at the grain-boundary trap electrons (which can be introduced by optical excitation or electron injection), interact with oxygen vacancies or interact with other protons segregated to the grain boundary. This is the approach we take in the following few paragraphs, however, it must be emphasized that the order in which the events occur may be different depending on the circumstances. For this discussion we consider that protons are mobile but that oxygen vacancies are immobile which corresponds to temperatures below 900 °C.[84]

We start by considering that a proton in the bulk diffuses toward the grain boundary. In the absence of any vacancies near the proton, site I (Fig. 7) is the most stable adsorption site, being 1.78 eV more favorable than the O^{2-} site in the bulk. In fact site I is also more stable than the O^{2-} site on the (001) surface which is due to the stabilizing electrostatic effect of nearby oxygen ions at the grain boundary. Figure 8 shows the corresponding electronic levels for the proton related defects. It shows that a proton in site I (denoted p_I) has an unoccupied level in the gap and therefore can trap an electron from the conduction band. On trapping an electron a H atom is formed, which is weakly adsorbed on the same O ion as the proton (H_I). The spin density for the H atom at the grain boundary is shown in Fig. 9(a). The calculated adsorption energy for H at the (001) surface is in agreement with previous calculations and experiment[33] therefore, our predictions of weak H adsorption at the grain boundary should be accurate.

Examining Fig. 8 one finds that the H atom at the grain boundary also has an unoccupied level in the gap. The H

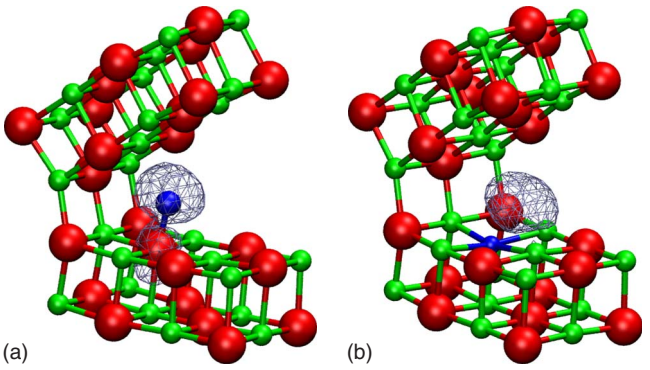

FIG. 9. (Color online) (a) Electron spin density associated with H atom at the grain boundary and with (b) a H_b^{2-} defect (see text for description). Isosurfaces correspond to 4×10^{-3} e Å^{-3}.

atom has an electron affinity (with respect to the vacuum level) of 2.51 eV and on trapping an electron a H_I^- defect is formed. The defect is stabilized by considerable structural relaxation: the H^- moves toward the center of the dislocation core and the opposite Mg ion relaxes toward it. The H^- ion has another unoccupied level in the gap but it is very shallow so further charging is unlikely.

Now let us consider what may happen if a proton diffuses to the boundary and finds itself close to an oxygen vacancy. We take the example of a single oxygen vacancy located in the most favorable site at the grain boundary [b in Fig. 1(b)]. Our calculations of the formation energy (Table III) show that protons are repelled from the positively charged vacancies (F^{2+} and F^+), however, protons do favorably bind to the neutral vacancy. The defect that is formed consists of a proton that sits in the center of the vacancy along with two electrons, which we refer to as H_b^-. This type of defect has been discussed previously for bulk MgO.[85–87] The formation of the H_b^- defect is described by the following reaction:

$$p_I + F_b^0 \leftrightarrow H_b^-(-2.49\ \text{eV}),$$

where the number in brackets is the reaction energy (the sign convention is that a negative number means the reaction is exothermic proceeding from left to right). We also checked other possible configurations which may be generated following interaction of a proton with a neutral vacancy. The first is the production of a H atom and a F^+ defect,

$$p_I + F_b^0 \leftrightarrow H_I + F_b^+(+1.49\ \text{eV}),$$

and the second is the production of a H^- ion and a F^{2+} defect,

$$p_I + F_b^0 \leftrightarrow H_I^- + F_b^{2+}(+2.90\ \text{eV}),$$

both of which are energetically unfavorable.

The electronic structure of the H_b^- defect is shown in Fig. 8. It has an unoccupied level in the gap and therefore can trap additional electrons. If a single electron is trapped, a paramagnetic defect is formed (H_b^{2-}), in which the unpaired electron is localized in the center of the dislocation core [an electron density isosurface is shown in Fig. 9(b)]. The same defect can be produced by H atom adsorption into a neutral oxygen vacancy, which is also energetically favorable:

$$H_I + F_b^0 \leftrightarrow H_b^{2-}(-2.28\ \text{eV}).$$

In this process, as H adsorbs into the vacancy, it separates into a proton, which remains in the vacancy and an electron, which is localized nearby. This parallels the adsorption of H near steps on the MgO surface[33,69] where the electrostatic potential of the proton stabilizes the localization of the electron nearby. We also checked the possibility that an electron could be transferred from the vacancy to the H atom adsorbed at the grain boundary forming an H^- ion and a F^+ defect, but find it is less favorable than the reaction above

$$H_I + F_b^0 \leftrightarrow H_I^- + F_b^+(-0.19\ \text{eV}).$$

However, the fact that this reaction is exothermic suggests that electron transfer occurs as a metastable precursor to the H_b^{2-} configuration.

Finally, we consider possible reactions that can occur between two proton defects at the grain boundary. Two H atoms can favorably react to form a hydrogen molecule

$$H_I + H_I \leftrightarrow H_2(-3.62\ \text{eV}).$$

Hydrogen molecules can also be formed by the reaction of a proton with a H_I^- defect,

$$p_I + H_I^- \leftrightarrow H_2(-1.77\ \text{eV}),$$

and by the reaction of a proton with a H_b^{2-} defect,

$$p_I + H_b^{2-} \leftrightarrow H_2 + F_b^+(-4.60\ \text{eV}).$$

We find that reaction of a H atom with a H_b^- defect forming a hydrogen molecule and a doubly charged oxygen vacancy is energetically unfavorable

$$p_I + H_b^- \leftrightarrow H_2 + F_b^{2+}(+3.63\ \text{eV}).$$

The reaction energies above show that hydrogen molecules are the likely product when protons segregate and electrons are introduced or indeed vice versa. The hydrogen molecule at the boundary is 1.03 eV less stable than the molecule in vacuum, therefore, there is a thermodynamic driving force for the hydrogen to escape into the ambient. Whether this can happen depends upon the availability of a diffusion path to the surface.

The g tensors for the paramagnetic proton defects have been calculated using the approach that was described previously and are shown in Table II. For H, we find that the g-tensor components increase going from the surface to the grain boundary and to the bulk, as was seen for F^+. The adsorption of H into a F^0 defect also produces a paramagnetic center and the g tensors for this defect is also shown in the table.

V. DISCUSSION AND CONCLUSIONS

The results presented in this paper show that oxygen vacancies and proton impurities readily segregate to grain boundaries in MgO and that their electronic properties are different to those in the bulk. As conduction-band electrons also favorably trap at grain boundaries,[57] this provides a mechanism for charge to build up specifically at grain

boundaries, for example, under irradiation or applied electrical voltage. These effects can have a number of important consequences for various applications which we now discuss.

Oxygen vacancy defects in electronic devices, such as Fe/MgO/Fe magnetic tunnel junctions, can provide states through which electrons can tunnel thereby reducing the effective barrier height of the insulator. The metal Fermi energy in such devices is often aligned midgap for common electrode materials [e.g., about 3.5 eV above the valence band for Fe (Ref. 88) or Co-Fe (Ref. 26)]. In this case, based on formation energies, we find O vacancies in the bulk and at grain boundaries can have different charge states (F^+ in the bulk and F^0 at grain boundaries). As the occupied level of F^0 lies below the metal Fermi energy, our results suggest that the primary defect responsible for reducing the barrier height of MgO-based magnetic tunnel junctions under small bias is F^+ in the bulk. This defect has an unoccupied level 4.44 eV above the MgO valence band (Fig. 6) or about 0.9 eV above the metal Fermi energy. This figure is consistent with recent transport measurements.[89]

Our results suggest that the trapping of electrons by proton impurities at grain boundaries leads to the formation of H atoms and molecules. Therefore, irradiation of polycrystalline MgO may provide a means to remove proton defects, forming hydrogen gas. In support of this idea, it has been observed previously that hydrogen filled voids can be formed in MgO polycrystals in a reducing atmosphere[90] and grain boundaries are suspected nucleation sites for these voids. It has also been noted that there is a correlation between cloudy hydrogen filled voids and strong H^- infrared absorption.[86] The production of hydrogen molecules provides an illustration of how electron trapping can modify ion diffusion. Protons at the grain boundary are bound to O ions and diffuse by hopping between O ions as lattice vibrations bring them closer together. However, once an electron is trapped, the H atom is much more mobile.

It is also interesting to consider that the order in which process occur can be different to those described above. For example, excess electrons can be trapped at the grain boundary following optical excitation or electrical injection. If the boundary acquires a net negative charge it will attract proton defects from the bulk, forming hydrogen related defects and hydrogen molecules. More generally, charge-induced changes in defect mobility may play a central role in dielectric breakdown processes, radiation damage, and in the operation of fuel cells.

Our calculations predict a stable H^{2-} defect can be formed at the grain boundary in MgO. This type of defect was previously studied in the bulk, both theoretically by DFT and experimentally by optical absorption, luminescence spectroscopy, and EPR.[86,87] It was proposed that the additional electron trapped by H^- should be associated with a nearby impurity rather then the H atom. This is because there was no detectable EPR signal and only a small change in the proton infrared mode. Here we find a similar situation where the electron is not trapped on the H atom, but inside the dislocation pipe. In other words, it is the grain boundary that provides the perturbation needed to stabilize the H^{2-} defect.

Various experimental methods can be used to probe the properties of the defects discussed in this paper. However, whether it possible to separate the signals from defects at the boundary from those in the bulk is a key question. For example, on the basis of our results for the g tensors of paramagnetic species, such as F^+, this would seem possible given high enough EPR resolution (i.e., 10 ppm or better). The relative intensity of bulk, surface, and grain boundary features in EPR spectra will depend on grain size and therefore could be used as a tool to characterize polycrystalline materials. By combining EPR measurements with optical excitation or electrical injection, the concentration of specific charged defects, such as H^{2-}, could be increased permitting their detection.

To summarize, we have calculated the electronic properties of oxygen vacancies, proton impurities, and their stable combinations at a grain boundary in MgO. The embedded cluster method which we employ represents an advance over previous interatomic potential methods as it is not limited to modeling only a single charge state. Our results show that oxygen vacancies and proton impurities segregated to grain boundaries can form a number of defects which can favorably trap electrons. As grain boundaries in polycrystalline metal-oxide materials are places where these defects favorably segregate, electrons can be preferentially trapped there following processes such as irradiation, optical excitation, or electrical injection. These issues are important for many technological applications of polycrystalline metal-oxide materials and this paper is the first to address them theoretically.

ACKNOWLEDGMENTS

Computer resources on the HPCx service were provided via our membership of the UK's HPC Materials Chemistry Consortium and funded by EPSRC (portfolio Grant No. EP/D504872). Additional computation time was provided by the London Centre for Nanotechnology and by UCL's research computing. K.P.M. is supported by the Grant-in-Aid for Creative Scientific Research (Grant No. 16GS0205) from the Japanese Ministry for Education, Culture, Sports, Science, and Technology and also by EPSRC Grant No. GR/S80080/01. We acknowledge useful discussions with Peter Sushko, Marshall Stoneham, Yuichi Ikuhara, and Gennadi Besurker.

*k.mckenna@ucl.ac.uk

[1] J. Maier, Solid State Ionics **131**, 13 (2000).

[2] P. Mondal, A. Klein, W. Jaegermann, and H. Hahn, Solid State Ionics **118**, 331 (1999).

[3] T. Suzuki, I. Kosacki, H. U. Anderson, and P. Colomban, J. Am. Ceram. Soc. **84**, 2007 (2001).

[4] I. Kosacki, H. U. Anderson, Y. Mizutani, and K. Ukai, Solid State Ionics **152-153**, 431 (2002).

[5] I. Kosacki, C. M. Rouleaub, P. F. Bechera, J. Bentleya, and D. H. Lowndesb, Solid State Ionics **176**, 1319 (2005).
[6] A. G. Evans, D. R. Mumm, J. W. Hutchinson, G. H. Meier, and F. S. Pettit, Prog. Mater. Sci. **46**, 505 (2001).
[7] D. R. Clarke, J. Am. Ceram. Soc. **82**, 485 (1999).
[8] H. Hilgenkamp and J. Mannhart, Rev. Mod. Phys. **74**, 485 (2002).
[9] X. Song, G. Daniels, D. M. Feldmann, A. Gurevich, and D. Larbalestier, Nature Mater. **4**, 470 (2005).
[10] V. Yanev, Mathias Rommel, Martin Lemberger, Silke Petersen, Brigitte Amon, Tobias Erlbacher, Anton J. Bauer, Heiner Ryssel, Albena Paskaleva, Wenke Weinreich, Christian Fachmann, Johannes Heitmann, and Uwe Schroeder, Appl. Phys. Lett. **92**, 252910 (2008).
[11] K. Kukli, M. Ritala, J. Sundqvist, J. Aarik, J. Lu, T. Sajavaara, M. Leskelä, and A. Hårsta, J. Appl. Phys. **92**, 5698 (2002).
[12] A. P. Sutton and R. W. Balluffi, *Interfaces in Crystalline Materials* (Oxford University Press, New York, 1995).
[13] Y. Yan, M. F. Chisholm, G. Duscher, A. Maiti, S. J. Pennycook, and S. T. Pantelides, Phys. Rev. Lett. **81**, 3675 (1998).
[14] T. Norby, M. Widerøe, R. Glöckner, and Y. Larring, Dalton Trans. **2004**, 3012.
[15] I. Balint and K.-i. Aika, J. Chem. Soc., Faraday Trans. **93**, 1797 (1997).
[16] P. Wynblatt, G. S. Rohrer, and F. Papillon, J. Eur. Ceram. Soc. **23**, 2841 (2003).
[17] Y. M. Chiang, A. F. Henriksen, and W. D. Kingery, J. Am. Ceram. Soc. **64**, 385 (1981).
[18] J. W. Osenbach and V. S. Stubican, J. Am. Ceram. Soc. **66**, 191 (1983).
[19] C. M. Osburn and R. W. Vest, J. Am. Ceram. Soc. **54**, 428 (1971).
[20] D. M. Duffy, J. Phys. C **19**, 4393 (1986).
[21] J. H. Harding, D. J. Harris, and S. C. Parker, Phys. Rev. B **60**, 2740 (1999).
[22] D. J. Harris, G. W. Watson, and S. C. Parker, Phys. Rev. B **64**, 134101 (2001).
[23] D. C. Sayle, C. R. A. Catlow, J. H. Harding, M. J. F. Healy, S. A. Maicaneanu, S. C. Parker, B. Slater, and G. W. Watson, J. Mater. Chem. **10**, 1315 (2000).
[24] J. H. Harding, Interface Sci. **11**, 81 (2003).
[25] P. W. Tasker, E. A. Colburn, and W. C. Mackrodt, J. Am. Ceram. Soc. **68**, 74 (1985).
[26] S. S. P. Parkin, C. Kaiser, A. Panchula, P. M. Rice, B. Hughes, M. Samant, and S.-H. Yang, Nature Mater. **3**, 862 (2004).
[27] T. J. Vink, A. R. Balkenende, R. G. F. A. Verbeek, H. A. M. van Hal, and S. T. de Zwart, Appl. Phys. Lett. **80**, 2216 (2002).
[28] B. Yoon, H. Häkkinen, U. Landman, A. S. Wörz, J.-M. Antonietti, S. Abbet, K. Judai, and U. Heiz, Science **307**, 403 (2005).
[29] J. Narayan, R. A. Weeks, and E. Sonder, J. Appl. Phys. **49**, 5977 (1978).
[30] T. Kizuka and N. Tanaka, Phys. Rev. B **56**, R10079 (1997).
[31] P. V. Sushko, A. L. Shluger, and C. R. A. Catlow, Surf. Sci. **450**, 153 (2000).
[32] P. V. Sushko, J. L. Gavartin, and A. L. Shluger, J. Phys. Chem. B **106**, 2269 (2002).
[33] M. Sterrer, T. Berger, O. Diwald, E. Knözinger, P. V. Sushko, and A. L. Shluger, J. Chem. Phys. **123**, 064714 (2005).
[34] K. P. McKenna, P. V. Sushko, and A. L. Shluger, J. Am. Chem. Soc. **129**, 8600 (2007).
[35] D. M. Saylor, A. Morawiec, and G. S. Rohrer, Acta Mater. **51**, 3663 (2003).
[36] T. Kizuka, M. Iijima, and N. Tanaka, Philos. Mag. A **77**, 413 (1998).
[37] G. W. Watson, E. T. Kelsey, N. H. de Leeuw, D. J. Harris, and S. C. Parker, J. Chem. Soc., Faraday Trans. **92**, 433 (1996).
[38] J. H. Harding and C. Noguera, Philos. Mag. Lett. **77**, 315 (1998).
[39] I. Milas, B. Hinnemann, and E. A. Carter, J. Mater. Res. **23**, 1494 (2008).
[40] I. Milas and E. A. Carter, J. Mater. Sci. **44**, 1741 (2009).
[41] M. M. Abraham, C. T. Butler, and Y. Chen, J. Chem. Phys. **55**, 3752 (1971).
[42] K. Lehovec, J. Chem. Phys. **21**, 1123 (1953).
[43] K. L. Kliewer and J. S. Koehler, Phys. Rev. **140**, A1226 (1965).
[44] J. R. Macdonald, D. R. Franceschetti, and A. P. Lehnen, J. Chem. Phys. **73**, 5272 (1980).
[45] J. Maier, Prog. Solid State Chem. **23**, 171 (1995).
[46] J. Jamnik, J. Maier, and S. Pejovnik, Solid State Ionics **75**, 51 (1995).
[47] R. Waser and R. Hagenbeck, Acta Mater. **48**, 797 (2000).
[48] H. Dabringhaus and M. F. Butman, J. Phys.: Condens. Matter **15**, 5801 (2003).
[49] K. Sasaki and J. Maier, J. Appl. Phys. **86**, 5422 (1999).
[50] J. Maier, Phys. Chem. Chem. Phys. **5**, 2164 (2003).
[51] B. D. Huey and D. A. Bonnell, Solid State Ionics **131**, 51 (2000).
[52] S. V. Kalinin, R. Shao, and D. A. Bonnell, J. Am. Ceram. Soc. **88**, 1077 (2005).
[53] V. F. G. Tull, Proc. R. Soc. London, Ser. A **206**, 1934 (1951).
[54] Y. Sato, T. Mizoguchi, F. Oba, M. Yodogawa, T. Yamamoto, and Y. Ikuhara, J. Mater. Sci. **40**, 3059 (2005).
[55] P. G. Mather, J. C. Read, and R. A. Buhrman, Phys. Rev. B **73**, 205412 (2006).
[56] M. Sterrer, E. Fischbach, T. Risse, and H.-J. Freund, Phys. Rev. Lett. **94**, 186101 (2005).
[57] K. P. McKenna and A. L. Shluger, Nature Mater. **7**, 859 (2008).
[58] I. Dawson, P. D. Bristowe, M.-H. Lee, M. C. Payne, M. D. Segall, and J. A. White, Phys. Rev. B **54**, 13727 (1996).
[59] S.-D. Mo, W. Y. Ching, and R. H. French, J. Phys. D **29**, 1761 (1996).
[60] M. Kim, G. Duscher, N. D. Browning, K. Sohlberg, S. T. Pantelides, and S. J. Pennycook, Phys. Rev. Lett. **86**, 4056 (2001).
[61] M. Imaeda, T. Mizoguchi, Y. Sato, H. S. Lee, S. D. Findlay, N. Shibata, T. Yamamoto, and Y. Ikuhara, Phys. Rev. B **78**, 245320 (2008).
[62] F. Oba, S. R. Nishitani, H. Adachi, I. Tanaka, M. Kohyama, and S. Tanaka, Phys. Rev. B **63**, 045410 (2001).
[63] C.-L. Liu, Phys. Status Solidi B **233**, 18 (2002).
[64] G. V. Lewis and C. R. A. Catlow, J. Phys. C **18**, 1149 (1985).
[65] E. Giamello, M. C. Paganini, D. M. Murphy, A. M. Ferrari, and G. Pacchioni, J. Phys. Chem. B **101**, 971 (1997).
[66] A. L. Shluger, C. R. A. Catlow, R. W. Grimes, and N. Itoh, J. Phys.: Condens. Matter **3**, 8027 (1991).
[67] A. L. Shluger, P. V. Sushko, and L. N. Kantorovich, Phys. Rev. B **59**, 2417 (1999).
[68] D. Ricci, G. Pacchioni, P. V. Sushko, and A. L. Shluger, J. Chem. Phys. **117**, 2844 (2002).
[69] D. Ricci, C. Di Valentin, G. Pacchioni, P. V. Sushko, A. L. Shluger, and E. Giamello, J. Am. Chem. Soc. **125**, 738 (2003).

[70] M. Chiesa, M. C. Paganini, E. Giamello, C. D. Valentin, and G. Pacchioni, Angew. Chem., Int. Ed. **42**, 1759 (2003).
[71] M. Chiesa, M. C. Paganini, G. Spoto, E. Giamello, C. D. Valentin, A. D. Vitto, and G. Pacchioni, J. Phys. Chem. B **109**, 7314 (2005).
[72] A. D. Becke, J. Chem. Phys. **98**, 5648 (1993).
[73] P. J. Stephens, F. J. Devlin, C. F. Chabalowski, and M. J. Frisch, J. Phys. Chem. **98**, 11623 (1994).
[74] J. Muscat, A. Wander, and N. M. Harrison, Chem. Phys. Lett. **342**, 397 (2001).
[75] P. E. Blöchl, Phys. Rev. B **50**, 17953 (1994).
[76] G. Kresse and J. Furthmüller, Phys. Rev. B **54**, 11169 (1996).
[77] G. Kresse and J. Furthmüller, Comput. Mater. Sci. **6**, 15 (1996).
[78] G. Henkelman, A. Arnaldsson, and H. Jónsson, Comput. Mater. Sci. **36**, 354 (2006).
[79] A. Alkauskas, P. Broqvist, and A. Pasquarello, Phys. Rev. Lett. **101**, 046405 (2008).
[80] M. Rohlfing, N.-P. Wang, P. Krüger, and J. Pollmann, Phys. Rev. Lett. **91**, 256802 (2003).
[81] C. Di Valentin, K. M. Neyman, T. Risse, M. Sterrer, E. Fischbach, H.-J. Freund, V. A. Nasluzov, G. Pacchioni, and N. Rösch, J. Chem. Phys. **124**, 044708 (2006).
[82] T. Norby and Y. Larring, Curr. Opin. Solid State Mater. Sci. **2**, 593 (1997).
[83] M. S. Mel'gunov, V. B. Fenelonov, E. A. Mel'gunova, A. F. Bedilo, and K. J. Klabunde, J. Phys. Chem. B **107**, 2427 (2003).
[84] Y. Chen, R. T. Williams, and W. A. Sibley, Phys. Rev. **182**, 960 (1969).
[85] M. M. Kuklja, E. V. Stefanovich, E. A. Kotomin, A. I. Popov, R. González, and Y. Chen, Phys. Rev. B **59**, 1885 (1999).
[86] V. M. Orera and Y. Chen, Phys. Rev. B **36**, 6120 (1987).
[87] R. González, M. A. Monge, J. E. Muñoz Santiuste, R. Pareja, Y. Chen, E. Kotomin, M. M. Kukla, and A. I. Popov, Phys. Rev. B **59**, 4786 (1999).
[88] K. D. Belashchenko, J. Velev, and E. Y. Tsymbal, Phys. Rev. B **72**, 140404(R) (2005).
[89] G. X. Miao, Y. J. Park, J. S. Moodera, M. Seibt, G. Eilers, and M. Münzenberg, Phys. Rev. Lett. **100**, 246803 (2008).
[90] A. Briggs, J. Mater. Sci. **10**, 737 (1975).